DRUG METABOLISM AND DISPOSITION

Supplemental Materials

A study on pharmacokinetics of bosentan with systems modeling, Part 1: translating systemic plasma concentration to liver exposure in healthy subjects

Rui Li, Mark Niosi, Nathaniel Johnson, David A. Tess, Emi Kimoto, Jian Lin, Xin Yang, Keith A. Riccardi, Sangwoo Ryu, Ayman F. El-Kattan, Tristan S. Maurer, Larry M. Tremaine, and Li Di

A physiologically based pharmacokinetics model for bosentan

Systemic blood model. The arterial blood, venous blood, and lung are lumped together as systemic blood, which is then split into systemic plasma and red blood cells (RBC). Due to potential nonlinear binding kinetics, instead of assuming constant plasma unbound fraction ($f_{u,p}$) or blood to plasma ratio ($R_{B/C}$), we use kinetic model to describe binding in plasma and red blood cells. As such, the binding in the plasma is modeled with mass balances of unbound concentration, bound concentration, and available binding site concentration (Equation 1 to 3)

$$\frac{dC_{unbound}}{dt} = -k_{on} \cdot C_{unbound} \cdot C_{available-site} + k_{off} \cdot C_{bound} \quad (1)$$

$$\frac{dC_{available-site}}{dt} = -k_{on} \cdot C_{unbound} \cdot C_{available-site} + k_{off} \cdot C_{bound} \quad (2)$$

$$\frac{dC_{bound}}{dt} = k_{on} \cdot C_{unbound} \cdot C_{available-site} - k_{off} \cdot C_{bound} \quad (3)$$

Similarly, the distribution in RBC is modeled with mass balances of unbound systemic RBC concentration, bound systemic RBC concentration, and available RBC binding site concentration. We assume that there is a passive permeation between RBC and plasma, hence the kinetics of $R_{B/P}$ depends on the binding in both plasma and RBC.

The target mediated drug disposition (TMDD) has been proposed in a previous study (Volz et al., 2017). Although it is easy to understand that target binding may change the distribution, it is hard to believe that the targets (i.e. endothelin receptors, ET) or their internalization can eliminate the compound without solid biological evidence. As such, in addition to the non-specific binding to the plasma protein for compound in the systemic plasma, specific binding to the ET has been added. Different from binding

to plasma and RBC proteins, the binding parameters to ET are optimized with other parameters by fitting clinical data.

For perfusion-limited tissue compartments, we assume that instantaneous equilibrium between tissue and unbound systemic plasma is limited by blood flow. Except for unbound plasma concentration, the other components in systemic blood do not interact with these tissues directly. On the other hand, all components in the systemic blood are connected with their counterparts in the liver and villi blood, except that we assume target binding in the liver and villi blood is minimal.

The final model (Equation 4 to 8) for systemic plasma incorporates circulation (e.g. the first row of Equation 4), binding to plasma protein (e.g. the second row of Equation 4), diffusion between plasma and RBC (e.g. the third row of Equation 4), and binding to ET (e.g. the forth row of Equation 4), while the model (Equation 9 to 11) for systemic RBC incorporates circulation, binding to RBC protein, and diffusion between plasma and RBC. In the following equations, *HCT* represents hematocrit; *V*, *C*, *Q*, and *T* represent volume, concentration, blood flow, and tissue; *UP*, *BP*, and *ASP* represent unbound plasma, bound plasma, and available binding sites in plasma; *BET* and *ASET* represent bound and unbound ET; *UR*, *BR*, and *ASR* represent unbound RBC, bound RBC, and available binding sites in RBC; $Kp_{,u}$ represents total tissue to unbound plasma concentration ratio; and $CL_{systemic,blood,pass}$ represents passive permeation between unbound systemic RBC and plasma, which is the product of permeability and estimated surface area.

The permeability is calculated as the ratio of SCHH $CL_{HEP,pass}$ (10.8 $uL \cdot min^{-1} \cdot mg^{-1}$) in Part 2 to an assumed hepatocyte surface area (2.30×10^9 $\mu m^2 \cdot mg^{-1}$) of 1 mg protein (i.e. 2.5×10^6 million cells), where we assume a hepatocyte is a sphere with a diameter of 17.1 μm. The volume of a single RBC is assumed to be 90 fL (Turgeon, 2017), while the volume of total RBC in systemic blood is 2.63 L (Table S1). Assuming that RBC is spherical, we can derive the total surface area of RBC in systemic blood as

2.57×10^{14} μm^2. Finally, $CL_{systemic,blood,pass}$ is determined as 1.12×10^{3} L·hour^{-1}. The values of $CL_{liver,blood,pass}$ and $CL_{villi,blood,pass}$ are calculated using the same approach, but with volume of RBC in liver and small intestine villi blood.

$$\begin{aligned}
&V_{systemic,plasma}\cdot\frac{dC_{systemic,UP}}{dt}\\
&=\left[Q_{liver,venous}\cdot C_{liver,UP,5}+\sum_{i=1}^{11}Q_{T,i}\cdot C_{T,i}/Kp_{uT,i}-Q_{total}\cdot C_{systemic,UP}\right]\cdot\left[1-HCT\right]\\
&-\left[k_{on,plasma}\cdot C_{systemic,UP}\cdot C_{systemic,ASP}-k_{off,plasma}\cdot C_{systemic,BP}\right]\cdot V_{systemic,plasma}\\
&-\left[C_{systemic,UP}-C_{systemic,UR}\right]\cdot CL_{systemic,blood,pass}\\
&-\left[k_{on,ET}\cdot C_{systemic,UP}\cdot C_{systemic,ASET}-k_{off,ET}\cdot C_{systemic,BET}\right]\cdot V_{systemic,plasma}
\end{aligned}\tag{4}$$

$$\begin{aligned}
&V_{systemic,plasma}\cdot\frac{dC_{systemic,BP}}{dt}\\
&=\left[Q_{liver,arterial}\cdot C_{liver,BP,5}-Q_{liver,arterial}\cdot C_{systemic,BP}\right]\cdot\left[1-HCT\right]\\
&+\left[k_{on,plasma}\cdot C_{systemic,UP}\cdot C_{systemic,ASP}-k_{off,plasma}\cdot C_{systemic,BP}\right]\cdot V_{systemic,plasma}
\end{aligned}\tag{5}$$

$$\begin{aligned}
&V_{systemic,plasma}\cdot\frac{dC_{systemic,ASP}}{dt}\\
&=\left[Q_{liver,arterial}\cdot C_{liver,ASP,5}-Q_{liver,arterial}\cdot C_{systemic,ASP}\right]\cdot\left[1-HCT\right]\\
&-\left[k_{on,plasma}\cdot C_{systemic,UP}\cdot C_{systemic,ASP}-k_{off,plasma}\cdot C_{systemic,BP}\right]\cdot V_{systemic,plasma}
\end{aligned}\tag{6}$$

$$\frac{dC_{systemic,ASET}}{dt}=k_{on,ET}\cdot C_{systemic,UP}\cdot C_{systemic,ASET}-k_{off,ET}\cdot C_{systemic,BET}\tag{7}$$

$$\frac{dC_{systemic,BET}}{dt}=-k_{on,ET}\cdot C_{systemic,UP}\cdot C_{systemic,ASET}+k_{off,ET}\cdot C_{systemic,BET}\tag{8}$$

$$\begin{aligned}
&V_{systemic,RBC}\cdot\frac{dC_{systemic,UR}}{dt}\\
&=\left[Q_{liver,arterial}\cdot C_{liver,UR,5}-Q_{liver,arterial}\cdot C_{venous,UR}\right]\cdot HCT\\
&-\left[k_{on,RBC}\cdot C_{systemic,UR}\cdot C_{venous,ASR}-k_{off,RBC}\cdot C_{systemic,BR}\right]\cdot V_{systemic,RBC}\\
&+\left[C_{systemic,UP}-C_{systemic,UR}\right]\cdot CL_{systemic,blood,pass}
\end{aligned}\tag{9}$$

$$V_{systemic,RBC} \cdot \frac{dC_{systemic,BR}}{dt} = \left[Q_{liver,arterial} \cdot C_{liver,BR,5} - Q_{liver,arterial} \cdot C_{systemic,BR} \right] \cdot HCT + \left[k_{on,RBC} \cdot C_{systemic,UR} \cdot C_{systemic,ASR} - k_{off,RBC} \cdot C_{systemic,BR} \right] \cdot V_{systemic,RBC} \quad (10)$$

$$V_{systemic,RBC} \cdot \frac{dC_{systemic,ASR}}{dt} = \left[Q_{liver,arterial} \cdot C_{liver,ASR,5} - Q_{liver,arterial} \cdot C_{venous,ASR} \right] \cdot HCT - \left[k_{on,RBC} \cdot C_{systemic,UR} \cdot C_{systemic,ASR} - k_{off,RBC} \cdot C_{systemic,BR} \right] \cdot V_{systemic,RBC} \quad (11)$$

Non-liver tissue distribution model. Perfusion-limited compartments are applied to non-liver tissues. The equilibrium tissue concentration is defined by in silico predicted Kp_u (i.e. total tissue to unbound plasma ratio) values (Rodgers and Rowland, 2006).

$$V_{T,i} \cdot \frac{dC_{T,i}}{dt} = \left[C_{systemic,UP} - C_{T,i} / Kp_{uT,i} \right] \cdot Q_{T,i} \cdot \left[1 - HCT \right] \quad (12)$$

It is unclear if in silico predicted Kp_u value could reasonably represent actual tissue distribution. As such, we employ an empirical scaling factor for the in silico Kp_u, which is optimized with other parameters in fitting clinical data. However, we find that data fitting and liver prediction do not change significantly with and without scaling factor for Kp_u. As such, this scaling factor is removed from the final model.

Liver model. Each liver blood sub-compartment is split into six components (i.e. unbound liver plasma concentration, bound liver plasma concentration, available binding site concentration in liver plasma, unbound liver RBC concentration, bound liver RBC concentration, and available binding site concentration in liver RBC). TMDD is ignored in the liver blood. The hepatic uptake, efflux, and passive diffusion mediate bosentan transport between unbound liver plasma (i.e. *UP*) and unbound liver

tissue (i.e. *UT*). One of five liver blood segments (i.e. the i^{th} segment) is presented here as an example (Equation 13 to 15 for liver plasma, and Equation 16 to 18 for liver RBC). In the following equations, $CL_{liver,blood,pass}$ represents passive permeation between unbound liver RBC and plasma, $CL_{liver,pass}$ represents passive diffusion between unbound liver plasma and unbound liver tissue, $k_{liver,uptake}$ and $k_{liver,efflux}$ represent active uptake and efflux rates, and $K_{M,liver,uptake}$ and $K_{M,liver,efflux}$ represent Michaelis-Menten constant.

$$
\begin{aligned}
& V_{liver,plasma,i}\frac{dC_{liver,UP,i}}{dt} \\
&= \left[C_{liver,UP,i\text{-}1} - C_{liver,UP,i}\right]\cdot Q_{liver,venous}\cdot\left[1-HCT\right] \\
&-\left[k_{on,plasma}\cdot C_{liver,UP,i}\cdot C_{liver,ASP,i} - k_{off,plasma}\cdot C_{liver,BP,i}\right]\cdot V_{liver,plasma,i} \\
&-\left[C_{liver,UP,i} - C_{liver,UR,i}\right]\cdot CL_{liver,blood,pass} \\
&-\left[C_{liver,UP,i} - C_{liver,UT,i}\right]\cdot CL_{liver,pass}/5 \\
&-C_{liver,UP,i}/\left[C_{liver,UP,i} + K_{M,liver,uptake}\right]\cdot k_{liver,uptake}/5 \\
&+C_{liver,UT,i}/\left[C_{liver,UT,i} + K_{M,liver,efflux}\right]\cdot k_{liver,efflux}/5
\end{aligned}
\tag{13}
$$

$$
\begin{aligned}
& V_{liver,plasma,i}\cdot\frac{dC_{liver,ASP,i}}{dt} \\
&= \left[C_{liver,ASP,i-1} - C_{liver,ASP,i}\right]\cdot\left[Q_{liver,arterial} + Q_{villi}\right]\cdot\left[1-HCT\right] \\
&-\left[k_{on,plasma}\cdot C_{liver,UP,i}\cdot C_{liver,ASP,i} - k_{off,plasma}\cdot C_{liver,BP,i}\right]\cdot V_{liver,plasma,i}
\end{aligned}
\tag{14}
$$

$$
\begin{aligned}
& V_{liver,plasma,i}\cdot\frac{dC_{liver,BP,i}}{dt} \\
&= \left[C_{liver,BP,i-1} - C_{liver,BP,i}\right]\cdot\left[Q_{liver,arterial} + Q_{villi}\right]\cdot\left[1-HCT\right] \\
&+\left[k_{on,plasma}\cdot C_{liver,UP,i}\cdot C_{liver,PP,i} - k_{off,plasma}\cdot C_{liver,BP,i}\right]\cdot V_{liver,plasma,i}
\end{aligned}
\tag{15}
$$

$$
\begin{aligned}
&V_{liver,RBC,i} \cdot \frac{dC_{liver,UR,i}}{dt} \\
&= \left[C_{liver,UR,i-1} - C_{liver,UR,i} \right] \cdot \left[Q_{liver,arterial} + Q_{villi} \right] \cdot HCT \\
&- \left[k_{on,RBC} \cdot C_{liver,UR,i} \cdot C_{liver,ASR,i} - \cdot k_{off,RBC} \cdot C_{liver,BR,i} \right] \cdot V_{liver,RBC,i} \\
&+ \left(C_{liver,UP,i} - C_{liver,UR,i} \right) \cdot CL_{liver,blood,pass}
\end{aligned} \tag{16}
$$

$$
\begin{aligned}
&V_{liver,RBC,i} \cdot \frac{dC_{liver,ASR,i}}{dt} \\
&= \left[C_{liver,ASR,i-1} - C_{liver,ASR,i} \right] \cdot \left[Q_{liver,arterial} + Q_{villi} \right] \cdot HCT \\
&- \left[k_{on,RBC} \cdot C_{liver,UR,i} \cdot C_{liver,ASR,i} - k_{off,RBC} \cdot C_{liver,BR,i} \right] \cdot V_{liver,RBC,i}
\end{aligned} \tag{17}
$$

$$
\begin{aligned}
&V_{liver,RBC,i} \cdot \frac{dC_{liver,BR,i}}{dt} \\
&= \left[C_{liver,BR,i-1} - C_{liver,BR,i} \right] \cdot \left[Q_{liver,arterial} + Q_{villi} \right] \cdot HCT \\
&+ \left[k_{on,RBC} \cdot C_{liver,UR,i} \cdot C_{liver,ASR,i} - k_{off,RBC} \cdot C_{liver,BR,i} \right] \cdot V_{liver,RBC,i}
\end{aligned} \tag{18}
$$

Within the liver tissue, the binding kinetics is explicitly modeled with k_{on} and k_{off} rates. Metabolism is modeled using metabolic rate and Machiens-Menton constant (i.e. $k_{liver,metabolism}$ and $K_{M,liver,metabolism}$). The biliary excretion is assumed to be zero based on the in vitro data (SCHH, Part 2 of this study published in a separated article) and in vivo observation that minimal compound is excreted into feces following intravenous dosing (Weber et al., 1999b). One of five liver tissue segments (i.e. the i^{th} segment) is presented here as an example (Equation 19 to 21). In these equations, *UT*, *BT*, and *AST* represent unbound tissue, bound tissue, and available binding sites in liver tissue. In Equation 19, the first row represents passive diffusion among tissue compartments, the second to the forth rows represent transport between unbound liver plasma and tissue, the fifth row represents metabolism, and the last row represents the binding kinetics. $E_{liver,induction,i}$ represents the induction effect in each segment which is explained below (Equation 32).

$$
\begin{aligned}
&V_{liver,tissue,i}\frac{dC_{liver,UT,i}}{dt}\\
&=\left[C_{liver,UT,i-1}+C_{liver,UT,i+1}-2\cdot C_{liver,UT,i}\right]\cdot CL_{liver,pass}/\left[5\times 2\right]\\
&+\left[C_{liver,UP,i}-C_{liver,UT,i}\right]\cdot CL_{liver,pass}/5\\
&+C_{liver,UP,i}/\left[C_{liver,UP,i}+K_{M,liver,uptake}\right]\cdot k_{liver,uptake}/5\\
&-C_{liver,UT,i}/\left[C_{liver,UT,i}+K_{M,liver,efflux}\right]\cdot k_{liver,efflux}/5\\
&-C_{liver,UT,i}/\left[C_{liver,UT,i}+K_{M,liver,metabolism}\right]\cdot k_{liver,metabolism}\cdot E_{liver,induction,i}/5\\
&+\left[k_{off,liver,tissue}\cdot C_{liver,BT,i}-k_{on,liver,tissue}\cdot C_{liver,UT,i}\cdot C_{liver,AST,i}\right]\cdot V_{liver,tissue,i}
\end{aligned}
\tag{19}
$$

$$
\frac{dC_{liver,AST,i}}{dt}=-k_{on,tissue}\cdot C_{liver,UT,i}\cdot C_{liver,AST,i}+k_{off,tissue}\cdot C_{liver,BT,i} \tag{20}
$$

$$
\frac{dC_{liver,BT,i}}{dt}=k_{on,tissue}\cdot C_{liver,UT,i}\cdot C_{liver,AST,i}-k_{off,tissue}\cdot C_{liver,BT,i} \tag{21}
$$

Absorption model. The oral absorption is modeled with a semi-mechanistic model. The orally administrated drug enters the model from the undissolved compartment, where it is transferred to the dissolved compartment with a first order rate constant (k_a) and scaled by fraction absorbed (F_a). The dissolved drug is transferred into the enterocyte also with the first order rate k_a. Since both k_a are parameter estimated by fitting clinical data, and are not uniquely distinguishable, we assume two k_a share the same value. We assume that 100% dissolved drug enters enterocyte in the model, because additional fraction parameter in this step would have the same impact on simulations as F_a. Once the drug enters enterocyte, it can be either metabolized, or transferred into villi blood by passive diffusion or active efflux. An enterocyte intracellular unbound fraction is applied and estimated by fitting clinical data with fitted other parameters. We assume that there is no active uptake from blood into enterocyte. Similar to blood in the systemic circulation and liver, villi blood is also split into six compartments to model binding in plasma and RBC (Equation 25 to 30).

$$\frac{dA_{undissolved}}{dt} = -k_a \cdot A_{undissolved} \tag{22}$$

$$\frac{dA_{dissolved}}{dt} = k_a \cdot A_{undissolved} \cdot F_a - k_a \cdot A_{dissolved} \tag{23}$$

$$\begin{aligned} & V_{enterocyte} \cdot \frac{dC_{enterocyte}}{dt} \\ & = k_a \cdot A_{dissolved} \\ & - C_{enterocyte} \cdot f_{u,enterocyte} \Big/ \left[C_{enterocyte} \cdot f_{u,enterocyte} + K_{M,gut,metabolism} \right] \cdot k_{enterocyte,metabolism} \cdot E_{eneterocyte,induction} \\ & - C_{enterocyte} \cdot f_{u,enterocyte} \cdot CL_{enterocyte,efflux} \\ & - \left[C_{enterocyte} \cdot f_{u,enterocyte} - C_{villi,UP} \right] \cdot CL_{enterocyte,pass} \end{aligned} \tag{24}$$

$$\begin{aligned} & V_{villi,plasam} \frac{dC_{villi,UP}}{dt} \\ & = \left[C_{systemic,UP} - C_{villi,UP} \right] \cdot Q_{villi} \cdot \left[1 - HCT \right] \\ & + \left[C_{enterocyte} \cdot f_{u,enterocyte} - C_{villi,UP} \right] \cdot CL_{enterocyte,pass} \\ & + C_{enterocyte} \cdot f_{u,enterocyte} \cdot CL_{enterocyte,efflux} \\ & - \left[C_{villi,UP} - C_{villi,UR} \right] \cdot CL_{villi,blood,pass} \end{aligned} \tag{25}$$

$$\begin{aligned} & V_{villi,plasma} \cdot \frac{dC_{villi,ASP}}{dt} \\ & = \left[C_{systemic,ASP} - C_{villi,ASP} \right] \cdot Q_{villi} \cdot \left[1 - HCT \right] \\ & - \left[k_{on,plasma} \cdot C_{villi,UP} \cdot C_{villi,ASP} - k_{off,plasma} \cdot C_{villi,BP} \right] \cdot V_{villi,plasma} \end{aligned} \tag{26}$$

$$\begin{aligned} & V_{villi,plasma} \cdot \frac{dC_{villi,BP}}{dt} \\ & = \left[C_{systemic,BP} - C_{villi,BP} \right] \cdot Q_{villi} \cdot \left[1 - HCT \right] \\ & + \left[k_{on,plasma} \cdot C_{villi,UP} \cdot C_{villi,ASP} - k_{off,plasma} \cdot C_{villi,BP} \right] \cdot V_{villi,plasma} \end{aligned} \tag{27}$$

$$
\begin{aligned}
&V_{villi,RBC} \cdot \frac{dC_{villi,UR}}{dt} \\
&= \left[C_{systemic,UR} - C_{villi,UR} \right] \cdot Q_{villi} \cdot HCT \\
&- \left[k_{on,RBC} \cdot C_{villi,UR} \cdot C_{villi,ASR} - k_{off,RBC} \cdot C_{villi,BR} \right] \cdot V_{villi,RBC} \\
&+ \left[C_{villi,UP} - C_{villi,UR} \right] \cdot CL_{villi,blood,pass}
\end{aligned} \tag{28}
$$

$$
\begin{aligned}
&V_{villi,RBC} \cdot \frac{dC_{villi,ASR}}{dt} \\
&= \left[C_{systemic,ASR} - C_{villi,ASR} \right] \cdot Q_{villi} \cdot HCT \\
&- \left[k_{on,RBC} \cdot C_{villi,UR} \cdot C_{villi,ASR} - k_{off,RBC} \cdot C_{villi,BR} \right] \cdot V_{villi,RBC}
\end{aligned} \tag{29}
$$

$$
\begin{aligned}
&V_{villi,RBC} \cdot \frac{dC_{villi,BR}}{dt} \\
&= \left[C_{systemic,BR} - C_{villi,BR} \right] \cdot Q_{villi} \cdot HCT \\
&+ \left[k_{on,RBC} \cdot C_{villi,UR} \cdot C_{villi,ASR} - k_{off,RBC} \cdot C_{villi,BR} \right] \cdot V_{villi,RBC}
\end{aligned} \tag{30}
$$

The total volume of all enterocytes is assumed to the same as the volume of the small intestine (i.e. 0.30 L (Shah and Betts, 2012)). The free fraction in the enterocyte is a parameter estimated by fitting clinical observation; hence it would adjust the intracellular free concentration if enterocyte volume was mis-specified. According to a previous study with oral dosed suspension, 30.2% of unchanged bosentan is excreted into feces (Weber et al., 1999b). As such, F_a can be approximated as 0.698 for suspension. Assuming different formulation of bosentan share the same hepatic extraction ratio (F_h) and fraction escaping gut metabolism (F_g), F_a will be proportional to plasma exposure after oral dosing. From $AUC_{0-\infty}$ of 24290 and 9022 ng·mL^{-1}·hour for 500 mg oral suspension and 125 mg tablet in tadalafil DDI study (Weber et al., 1999b; Wrishko et al., 2008), we can derive bosentan F_a in tadalafil DDI study as one. Similarly, F_a is estimated to be one for 125 mg and 500 mg tablets with high fat meal based on reported $AUC_{0-\infty}$ of 8791 and 43199 ng·mL^{-1}·hour (NDA-21-290, 2001; Dingemanse et al., 2002); 0.973 for 62.5 mg tablet based on AUC of 4234 ng·mL^{-1}·hour in ketoconazole DDI study (van

Giersbergen et al., 2002); 0.786, 0.991, and 0.909 for 100, 200, and 500 mg tablets based on $AUC_{0-\infty}$ of 5469, 13800, and 31640 ng·mL^{-1}·hour in a multiple ascending oral dose study (Weber et al., 1999c); and 0.736 for 500 mg tablets based on reported $AUC_{0-\infty}$ of 25600 ng·mL^{-1}·hour in a multiple oral dose study (Weber et al., 1999c). In the warfarin DDI study (Weber et al., 1999a), since bosentan pharmacokinetics is not reported, we have to assume that F_a for 500 mg tablet here is the average of 0.909 and 0.736 (i.e. 0.823).

The metabolic rate in the enterocyte ($k_{enterocyte,metabolism}$) is scaled from rate in the liver ($k_{liver,metabolism}$). Based on a human hepatocyte study performed in this study, CYP3A and 2C9 represent 70% and 10% of total hepatic metabolism. As such, from the value of $k_{liver,metabolism}$, the metabolic rates for hepatic CYP3A and 2C9 can be calculated as $k_{liver,metabolism} \times 0.7$ and $k_{liver,metabolism} \times 0.1$. Using human liver microsome assays, the abundances of CYP3A and 2C9 in the human liver have been reported to be 70.8 and 130.3 pmol·mg^{-1} (the averaged values from (Groer et al., 2014; Nakamura et al., 2016)). Assuming liver weight is 1.69×10^3 g (Shah and Betts, 2012) and microsomal protein (mg) per gram of liver (MPPGL) of 45, the specific metabolic rate for CYP3A and 2C9 are $k_{liver,metabolism} \times 0.7 / (70.8 \times 45 \times 1.69\times10^3)$ and $k_{liver,metabolism} \times 0.1 / (130.3 \times 45 \times 1.69\times10^3)$. Using human intestinal microsome assays, the abundances of CYP3A and 2C9 in the human small intestine have been reported to be 22.5 and 3.61 pmol·mg^{-1} (the averaged values from (Groer et al., 2014; Nakamura et al., 2016)). Assuming small intestine weight is 3.74×10^2 g (Shah and Betts, 2012) and microsomal protein (mg) per gram of intestine (MPPGI) of 20.6, the metabolic rate for CYP3A and 2C9 are $k_{liver,metabolism} \times 0.7 / (70.8 \times 45 \times 1.69 \times 10^3) \times (22.5 \times 20.6 \times 3.74\times10^2)$ and $k_{liver,metabolism} \times 0.1 / (130.3 \times 45 \times 1.69 \times 10^3) \times (3.61 \times 20.6 \times 3.74\times10^2)$. As a result, assuming that $k_{enterocyte,metabolism}$ is assumed to be the sum of CYP3A and 2C9 rates in the small intestine, the ratio of $k_{enterocyte,metabolism}$ to $k_{liver,metabolism}$ is 0.0260. Based on estimate $k_{liver,metabolism}$ value of 2.12×10^6 nmol·hour^{-1}, the value of $k_{enterocyte,metabolism}$ is 5.52×10^4 nmol·hour^{-1}.

Induction model. A turnover model is developed to describe in vivo CYP induction effect ($E_{induction}$), where $k_{synthesis}$ and $k_{degradatin}$ represent CYP synthesis and degradation rates. $k_{degradatin}$ is calculated as natural logarithm of 2 divided by CYP half-life. Multiple half-life values for CYP has been published, we pick the approach relying on the inactivation of CYP in clinical study. Induction is a relatively slow process, as such, the estimated half-life could be confounded by the residual effect of inducer even though inducer has been cleared from the body. On the other hand, inactivation is relatively fast. As far as the half-life of inactivator is short enough, the estimated half-life is minimally confounded. $k_{synthesis}$ is set to the same as $k_{degradatin}$ in order to keep base level of $E_{induction}$ at one in the absence of inducer. Five liver tissue segments and enterocyte have independent $E_{induction}$ calculation depending on unbound drug concentration in those tissues. The metabolic rates in liver tissue and gut are scaled by $E_{induction}$. In the absence of inducer, the $E_{induction}$ is a constant of one without affecting metabolism

$$\begin{aligned}&\frac{dE_{liver,induction,i}}{dt}\\&= k_{liver,synthesis}\cdot E_{max,liver,induction}\cdot\frac{C_{liver,UT,i}}{C_{liver,UT,i}+EC_{50,liver,induction}}\\&+k_{liver,synthesis}-k_{liver,degradation}\cdot E_{liver,induction,i}\end{aligned} \tag{31}$$

$$\begin{aligned}&\frac{dE_{enterocyte,induction}}{dt}\\&= k_{enterocyte,synthesis}\cdot E_{max,enterocyte,induction}\cdot\frac{C_{enterocyte}\cdot f_{u,enterocyte}}{C_{enterocyte}\cdot f_{u,enterocyte}+EC_{50,enterocyte,induction}}\\&+k_{enterocyte,synthesis}-k_{enterocyte,degradation}\cdot E_{enterocyte,induction}\end{aligned} \tag{32}$$

Victim model. A reduced PBPK model is developed for the drugs co-dosed with bosentan. Only systemic plasma, well-stirred liver, and empirical absorption compartments are included in this model

(Equation 34 to 36). In the following equations, $V_{central}$, Kp_{liver}, $R_{B/P}$, $f_{u,p}$, and CL_{liver} represent volume of central compartment, liver tissue to plasma partition coefficient, blood to plasma ratio, unbound fraction in plasma, and intrinsic hepatic clearance mediated by metabolism. $E_{liver,induction,i}$ values from five liver segments in bosentan model are averaged and used to scale CL_{liver} of victim compounds. Unfortunately, for victim drugs, there are not enough data to separate gut metabolism from absorption, hence induction is modeled implicitly as different F_aF_g values in the presence and absence of bosentan.

$$V_{central,victim} \cdot \frac{dC_{system,victim}}{dt} = \left[C_{liver,victim} / Kp_{liver,victim} \cdot R_{B/P,victim} - C_{system,victim} \right] \cdot Q_{liver,venous} \quad (33)$$

$$\begin{aligned} V_{liver,tissue} \cdot \frac{dC_{liver,victim}}{dt} &= \left[C_{system,victim} - C_{liver,victim} / Kp_{liver,victim} \cdot R_{B/P,victim} \right] \cdot Q_{liver,venous} \\ &- C_{liver,victim} / Kp_{liver,victim} \cdot f_{u,p,victim} \cdot CL_{liver,victim} \cdot E_{liver,induction} \\ &+ k_{a,victim} \cdot A_{absorption,victim} \cdot F_aF_{g,victim} \end{aligned} \quad (34)$$

$$\frac{dA_{absorption,victim}}{dt} = -k_{a,victim} \cdot A_{absorption,victim} \quad (35)$$

The physiological parameters in victim models have the same values as those in bosentan model. Kp_{liver} is calculated with in silico method as mentioned above. $R_{B/P}$ and $f_{u,p}$ are fixed at in house determined values. $V_{central}$, CL_{liver} and k_a are estimated by fitting clinical data of victim drugs in the absence of bosentan. S- and R-warfarin are fitted independently assuming racemic dosing include equal amount of equal amounts of left- and right-handed enantiomers, however to simplify the problem, we ignored potential inter-conversion between the two compounds after dosing. F_aF_g in the absence of bosentan is arbitrarily fixed at one as because the value of this parameter will not affect our interpretation of data.

On the other hand, F_aF_g values in the presence of bosentan are estimated by fitting clinical data, simultaneously with parameters of bosentan.

BSEP, MRP, NTCP inhibition. Simple competitive inhibition on four transporters is calculated independently based on simulated unbound bosentan concentrations. Because it is unclear if inhibition is driven by intracellular or extracellular bosentan, we have tried two scenarios with either predicted unbound liver tissue or liver plasma (not systemic plasma) concentration. Because the impact of these transporters on bosentan disposition is unclear, hence their inhibition is included in the PBPK model assuming minimal impact on bosentan exposure.

Parameter optimization and predicting liver exposure. Parameter estimation is performed with a previously developed numerical global optimizer (i.e. differential evolution, http://www1.icsi.berkeley.edu/~storn/code.html). MCMC (Markov chain Monte Carlo) toolbox for MATLAB (http://helios.fmi.fi/~lainema/mcmc/) is used to quantify the uncertainty. Starting from the globally optimized parameter values, the toolbox can provide ranges of parameter values that are able to reasonably describe the data. We randomly sample 1000 set of parameter values from all values (8×10^5 sets) identified from MCMC that can adequately describe plasma data. 1000 simulations using sampled parameter values are generated, such that uncertainty in parameter estimation is reflected in simulations.

A mechanistic model to analyze in vitro plasma free fraction and blood to plasma ratio data

The model includes concentrations of unbound compound ($C_{plasma,U}$), bound compound ($C_{plasma,B}$), and protein available for binding ($C_{plasma,P}$) in the plasma, as well as unbound compound ($C_{RBC,U}$), bound compound ($C_{RBC,B}$), and protein available for binding ($C_{RBC,P}$) in the red blood cells (RBC). Assuming the binding between compound and protein is non-specific in both plasma and blood, the mass balances are given as below.

$$\frac{dC_{plasma,U}}{dt} = -k_{on,plasma} \cdot C_{plasma,U} \cdot C_{plasma,P} + k_{off,plasma} \cdot C_{plasma,B} + \frac{CL_{blood,pass}}{V_{plasma}} \cdot \left[C_{RBC,U} - C_{plasma,U} \right] \tag{36}$$

$$\frac{dC_{plasma,B}}{dt} = k_{on,plasma} \cdot C_{plasma,U} \cdot C_{plasma,P} - k_{off,plasma} \cdot C_{plasma,B} \tag{37}$$

$$\frac{dC_{plasma,P}}{dt} = -k_{on,plasma} \cdot C_{plasma,U} \cdot C_{plasma,P} + k_{off,plasma} \cdot C_{plasma,B} \tag{38}$$

$$\frac{dC_{RBC,U}}{dt} = -k_{on,RBC} \cdot C_{RBC,U} \cdot C_{RBC,P} + k_{off,RBC} \cdot C_{RBC,B} - \frac{CL_{blood,pass}}{V_{plasma}} \cdot \left[C_{RBC,U} - C_{plasma,U} \right] \tag{39}$$

$$\frac{dC_{RBC,B}}{dt} = k_{on,RBC} \cdot C_{RBC,U} \cdot C_{RBC,P} - k_{off,RBC} \cdot C_{RBC,B} \tag{40}$$

$$\frac{dC_{RBC,P}}{dt} = -k_{on,RBC} \cdot C_{RBC,U} \cdot C_{RBC,P} + k_{off,RBC} \cdot C_{RBC,B} \tag{41}$$

$$f_{u,p} = \frac{C_{plasma,U}}{C_{plasma,U} + C_{plasma,B}} \tag{42}$$

$$
\begin{aligned}
R_{B/P} &= \frac{C_{blood}}{C_{plasma}} \\
&= \frac{C_{RBC} \cdot V_{RBC} + C_{plasma} \cdot V_{plasma}}{V_{blood} \cdot C_{plasma}} \\
&= \frac{C_{RBC,U} + C_{RBC,B}}{C_{plasma,U} + C_{plasma,B}} \cdot HCT + \left[1 - HCT\right]
\end{aligned}
\tag{43}
$$

HCT (i.e. hematocrit, the volume percentage of red blood cells in blood) is determined in the experiments. Given the data are not enough to estimate values for all binding kinetic parameters, association rates ($k_{on,plasma}$ and $k_{on,RBC}$) are fixed at 10^9 $mol^{-1} \cdot sec^{-1}$ assuming the reaction is limited by diffusion (Alberty and Hammes, 1958). The dissociation rates ($k_{off,plasma}$ and $k_{off,RBC}$), initial conditions for $C_{plasma,P}$ and $C_{plasma,P}$ are estimated by fitting observed $R_{B/P}$ and $f_{u,p}$ at different compound concentrations.

The data used for parameter estimation are presented in Figure S1. The estimated k_{off} rates and the concentration of binding sites are given in the Table 2.

In vitro induction assay and modeling

The induction assay was performed as following. Media free fraction ($f_{u,inc}$ 0.38) was measured to account for the binding due to bovine serum albumin in the media. We assume that intracellular concentration of bosentan in the induction assay is the same as that in the sandwich cultured human hepatocyte (SCHH) assay. As such, the intracellular concentration is simulated with model structure and parameter values published in an SCHH study (presented in Part 2 of this study, which is published in a separated article). To validate this assumption, we measure and simulate the intracellular concentration at 24 hours after initiating the induction assay. The difference between measured concentration and simulation is less than 2 fold, within the variability of the assay.

The turnover model described above for in vivo induction is used to estimate E_{max} and EC_{50} for CYP induction assay, except that the effect is driven by the unbound intracellular concentration simulated with SCHH model. Data from different hepatocyte lots are simultaneously model with shared EC_{50} but specific E_{max} for each lot.

In vitro cytochrome P450 (CYP) reaction phenotyping assay

The assay is performed as described previously using suspension human hepatocyte and selective inhibitors (Yang et al., 2016). The selective CYP 2C9 inactivator (i.e. tienilic acid) and 3A inactivator (i.e. troleandomycin) lead to 10% and 70% inhibition, respectively.

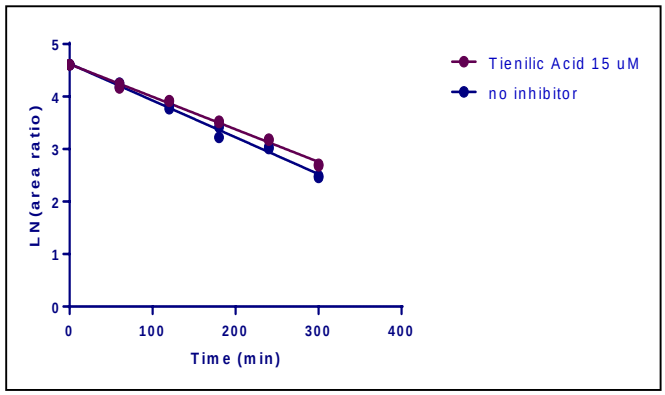

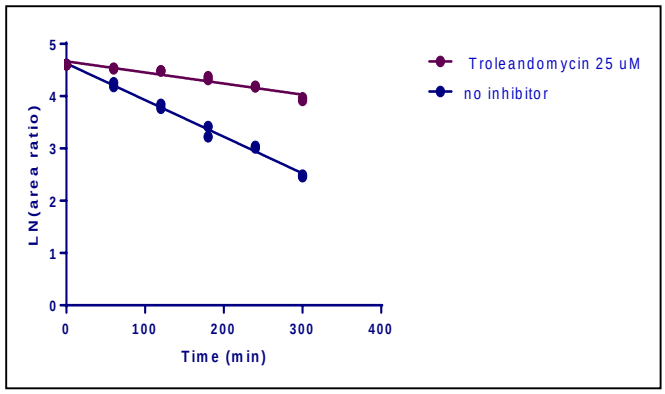

Table S1. Values for physiological parameters.

Tissue	Blood flow ($L \cdot hour^{-1} \cdot kg^{-1}$)	Volume ($L \cdot kg^{-1}$)
Adipose	0.222	0.143
Bone	0.216	0.124
Brain	0.6	0.0207
Gut [2]	0.558	0.0258
Villi blood [3]	0.256	0.000157
Heart	0.128	0.0038
Kidney	0.942	0.0044
Liver blood (arterial) [4]	0.266	0.00468
Liver tissue	-	0.0241
Muscle	0.642	0.429
Pancreas	0.114	0.0012
Skin	0.258	0.111
Spleen	0.066	0.0027
Systemic blood [5]	-	0.0723
Remaining [6]	0.0024	0.0288
Total [7]	4.26	1

1. All the values (except for those noted below) are calculated based on a previous publication (Peters, 2012).
2. The gut volume is calculated as the sum of the reported values for gut and stomach. Its blood flow is the sum of the reported values for gut and stomach minus villi blood flow.
3. Human villi blood flow is reported by (Yang et al., 2007). Shah and Betts reported the small intestine blood volume as 0.000157 $L \cdot kg^{-1}$ (Shah and Betts, 2012). We assume that this volume is the same as villi blood volume.
4. The arterial liver blood flows are calculated by removing gut, pancreas, and spleen values from reported liver values. Shah and Betts report the liver blood volumes (Shah and Betts, 2012).
5. The systemic blood volumes are the sums of the reported venous and arterial volumes minus liver blood volumes. HCT value (i.e. 0.52) is determined experimentally in house to separate blood volumes into RBC and plasma volumes.

6. The values for the rest of body are calculated to keep the mass balance.
7. The total blood flows (i.e. cardiac outputs) are the reported lung blood flows for monkey and rat, and the sum of all report blood flows excluding lung for human.

Table S2. The list of parameters with fixed values in victim model.

Parameter	Unit	Value	Source	Parameter	Unit	Value	Source
			Tadalafil				
k_a	$hour^{-1}$	0.629	See comment below	$R_{B/P}$		1.39	In house
F_aF_g		1	Arbitrarily fixed	$f_{u,p}$		0.06	In house
$V_{central}$	L	65.4	See comment below	Kp_{liver}		0.6	In silico predicted
CL_{liver}	$L\cdot hour^{-1}$	70.4	See comment below				
			S-warfarin				
k_a	$hour^{-1}$	0.641	See comment below	$R_{B/P}$		0.63	In house
F_aF_g		1	(Holford, 1986)	$f_{u,p}$		0.012	In house
$V_{central}$	L	10.7	See comment below	Kp_{liver}		0.09	In silico predicted
CL_{liver}	$L\cdot hour^{-1}$	9.99	See comment below				
			R-warfarin				
k_a	$hour^{-1}$	0.493	See comment below	$R_{B/P}$		0.63	In house
F_aF_g		1	(Holford, 1986)	$f_{u,p}$		0.012	In house
$V_{central}$	L	8.93	See comment below	Kp_{liver}		0.09	In silico predicted
CL_{liver}	$L\cdot hour^{-1}$	7.23	See comment below				

Values of k_a, $V_{central}$, and CL_{liver} are estimated by fitting clinical data listed in Table 1.

Figure S1. Observed (Marker) and fitted (solid line) human plasma free fraction (A) and blood to plasma ratio (B). In subplot (B), blue and red represent measurement at 1 and 3 hours.

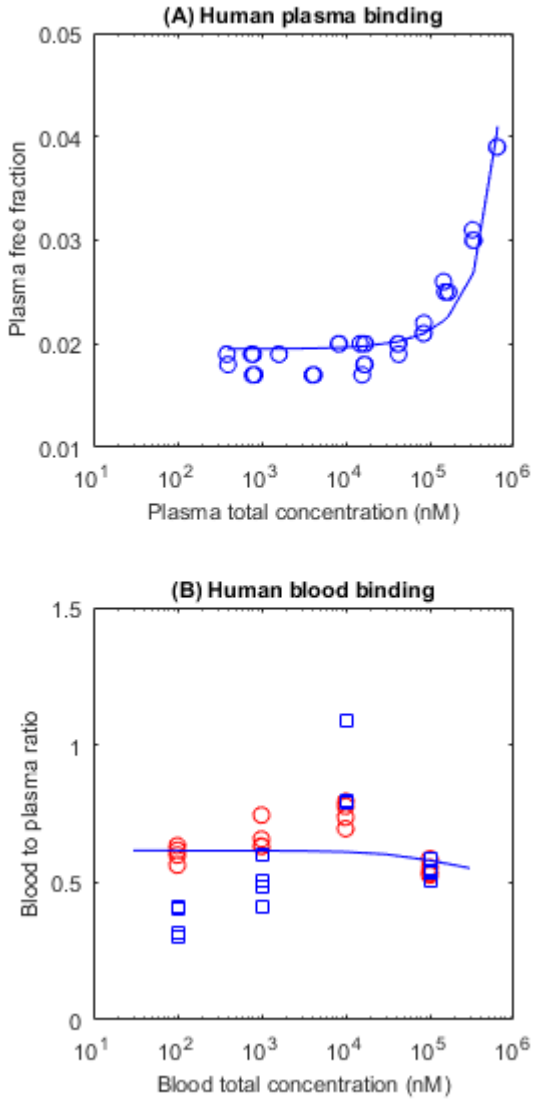

Figure S2. Observed (markers) and simulated (solid lines) induction effect of CYP3A4 (A and C) and 2B6 (B and D) due to bosentan. Subplots (A) and (B) represent activity measurements, while subplots (C) and (D) represent mRNA measurements. Red, blue, and black represent hepatocyte lots HC7-4, HH1025, and FOS.

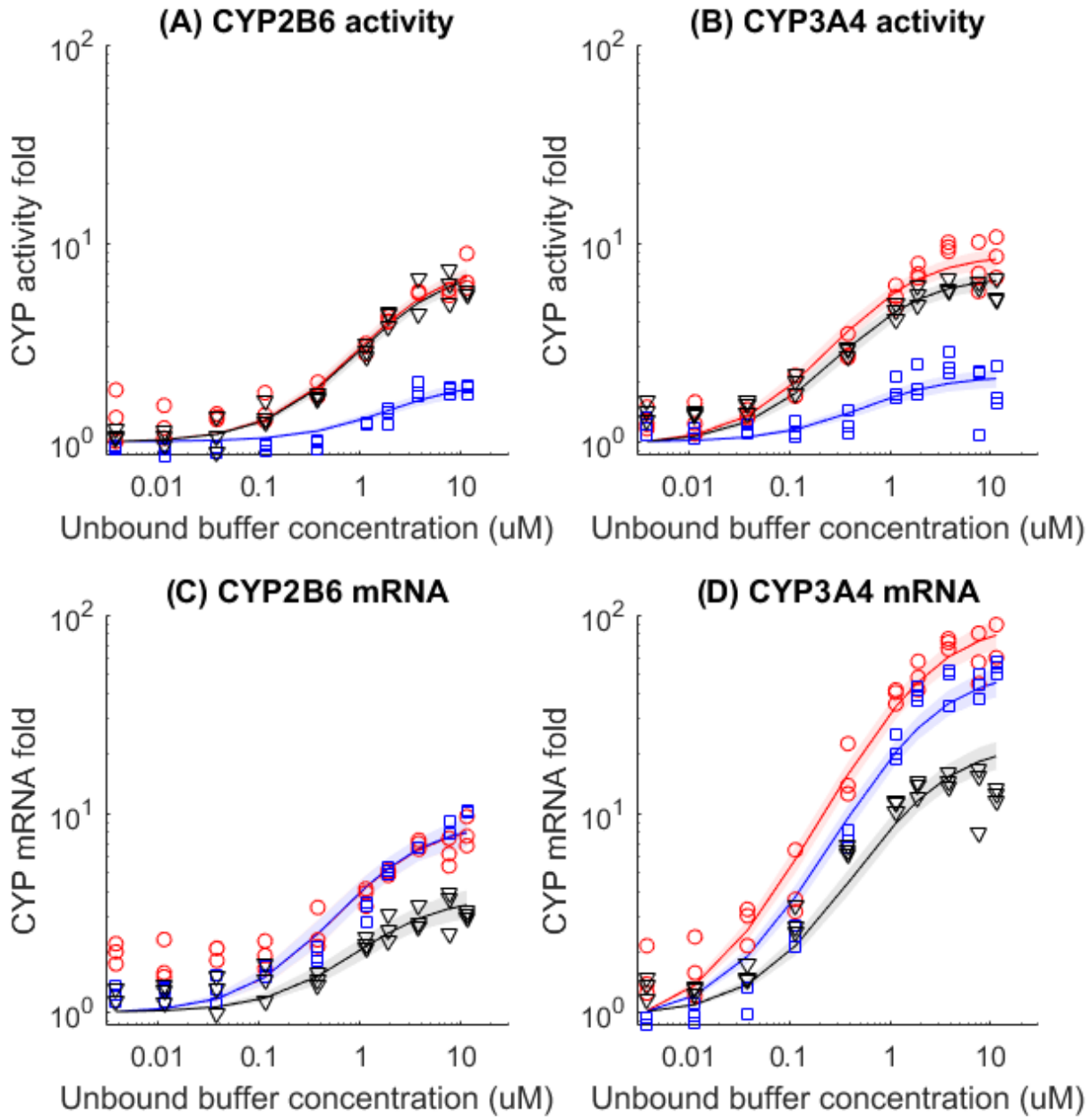

Reference

Alberty RA and Hammes GG (1958) Application of the Theory of Diffusion-controlled Reactions to Enzyme Kinetics. *The Journal of Physical Chemistry* **62:**154-159.

Dingemanse J, Bodin F, Weidekamm E, Kutz K, and van Giersbergen P (2002) Influence of food intake and formulation on the pharmacokinetics and metabolism of bosentan, a dual endothelin receptor antagonist. *J Clin Pharmacol* **42:**283-289.

Groer C, Busch D, Patrzyk M, Beyer K, Busemann A, Heidecke CD, Drozdzik M, Siegmund W, and Oswald S (2014) Absolute protein quantification of clinically relevant cytochrome P450 enzymes and UDP-glucuronosyltransferases by mass spectrometry-based targeted proteomics. *J Pharm Biomed Anal* **100:**393-401.

Holford NHG (1986) Clinical Pharmacokinetics and Pharmacodynamics of Warfarin. *Clinical Pharmacokinetics* **11:**483-504.

Nakamura K, Hirayama-Kurogi M, Ito S, Kuno T, Yoneyama T, Obuchi W, Terasaki T, and Ohtsuki S (2016) Large-scale multiplex absolute protein quantification of drug-metabolizing enzymes and transporters in human intestine, liver, and kidney microsomes by SWATH-MS: Comparison with MRM/SRM and HR-MRM/PRM. *Proteomics* **16:**2106-2117.

NDA-21-290 (2001) Clinical pharmacology and biopharmaceutics review. *Center for Drug Devaluation and Research, US Food and Drug Administration*.

Peters SA (2012) Appendices, in: *Physiologically-Based Pharmacokinetic (PBPK) Modeling and Simulations*, pp 407-421, John Wiley & Sons, Inc.

Rodgers T and Rowland M (2006) Physiologically based pharmacokinetic modelling 2: predicting the tissue distribution of acids, very weak bases, neutrals and zwitterions. *J Pharm Sci* **95:**1238-1257.

Shah DK and Betts AM (2012) Towards a platform PBPK model to characterize the plasma and tissue disposition of monoclonal antibodies in preclinical species and human. *J Pharmacokinet Pharmacodyn* **39:**67-86.

Turgeon ML (2017) *Clinical hematology: theory & procedures*. Wolters Kluwer, Philadelphia, PA.

van Giersbergen PL, Halabi A, and Dingemanse J (2002) Single- and multiple-dose pharmacokinetics of bosentan and its interaction with ketoconazole. *Br J Clin Pharmacol* **53:**589-595.

Volz AK, Krause A, Haefeli WE, Dingemanse J, and Lehr T (2017) Target-Mediated Drug Disposition Pharmacokinetic-Pharmacodynamic Model of Bosentan and Endothelin-1. *Clin Pharmacokinet*.

Weber C, Banken L, Birnboeck H, and Schulz R (1999a) Effect of the endothelin-receptor antagonist bosentan on the pharmacokinetics and pharmacodynamics of warfarin. *J Clin Pharmacol* **39:**847-854.

Weber C, Gasser R, and Hopfgartner G (1999b) Absorption, excretion, and metabolism of the endothelin receptor antagonist bosentan in healthy male subjects. *Drug Metab Dispos* **27:**810-815.

Weber C, Schmitt R, Birnboeck H, Hopfgartner G, Eggers H, Meyer J, van Marle S, Viischer HW, and Jonkman JH (1999c) Multiple-dose pharmacokinetics, safety, and tolerability of bosentan, an endothelin receptor antagonist, in healthy male volunteers. *J Clin Pharmacol* **39:**703-714.

Wrishko RE, Dingemanse J, Yu A, Darstein C, Phillips DL, and Mitchell MI (2008) Pharmacokinetic Interaction Between Tadalafil and Bosentan in Healthy Male Subjects. *The Journal of Clinical Pharmacology* **48:**610-618.

Yang J, Jamei M, Yeo KR, Tucker GT, and Rostami-Hodjegan A (2007) Prediction of intestinal first-pass drug metabolism. *Curr Drug Metab* **8:**676-684.

Yang X, Atkinson K, and Di L (2016) Novel Cytochrome P450 Reaction Phenotyping for Low-Clearance Compounds Using the Hepatocyte Relay Method. *Drug Metab Dispos* **44:**460-465.